Materials and electrical characterization of Er(Si1-xGex)(2-y) films formed on Si1-xGex(001) (x=0-0.3) via rapid thermal annealing

Setiawan, Y.; Tan, Eu Jin; Pey, Kin Leong; Chi, Dong Zhi; Lee, Pooi See; Hoe, Keat Mun

2007

Tan, E. J., Pey, K. L., Chi, D. Z., Lee, P. S., Setiawan, Y., & Hoe, K. M. (2008). Materials and electrical characterization of Er(Si1-xGex)(2-y) films formed on Si1-xGex(001) (x=0-0.3) via rapid thermal annealing. Journal of the Electrochemical Society, 155(1).

https://hdl.handle.net/10356/94039

https://doi.org/10.1149/1.2800761

Journal of The Electrochemical Society, **155** (1) H26-H30 (2008)
0013-4651/2007/155(1)/H26/5/$23.00 © The Electrochemical Society

Materials and Electrical Characterization of $Er(Si_{1-x}Ge_x)_{2-y}$ Films Formed on $Si_{1-x}Ge_x(001)$ (x = 0–0.3) via Rapid Thermal Annealing

E. J. Tan,[a,b,d,z] K. L. Pey,[a] D. Z. Chi,[b] P. S. Lee,[c] Y. Setiawan,[c] and K. M. Hoe[d]

[a]*School of Electrical and Electronic Engineering, and* [c]*School of Materials Science and Engineering, Nanyang Technological University, Singapore 639798*
[b]*Institute of Materials Research Engineering, Singapore 117602*
[d]*Institute of Microelectronics, Singapore 117685*

We studied erbium germanosilicide films formed on relaxed p-type $Si_{1-x}Ge_x(100)$ (x = 0–0.3) virtual substrates by conventional rapid thermal annealing (RTA) at temperatures of 500–700°C. Two dimensional X-ray diffraction and pole figure measurements revealed that the silicide films formed were epitaxial $Er(Si_{1-x}Ge_x)_{2-y}$ with orientation relationship $Er(Si_{1-x}Ge_x)_{2-y}(1\bar{1}00)$-$[0001] \parallel Si_{1-x}Ge_x(001)[110]$ or $Er(Si_{1-x}Ge_x)_{2-y}(1\bar{1}00)[0001] \parallel Si_{1-x}Ge_x(001)[\bar{1}10]$. Schottky barrier height, ϕ_{Bp}, of the $Er(Si_{1-x}Ge_x)_{2-y}/p - Si_{1-x}Ge_x(100)$ contact was found to decrease from 0.79 to 0.62 eV with increasing Ge (from 0 to 30%), implying a slight increase in its barrier height for electrons, ϕ_{Bneff}, from 0.33 to 0.37 eV.
 [DOI: 10.1149/1.2800761]

Manuscript submitted August 6, 2007; revised manuscript received September 24, 2007.
Available electronically November 7, 2007.

Silicon germanium is being used in high-speed complementary metal oxide semiconductors (CMOSs) in the source/drain region for mobility enhancement by inducing channel strain,[1] and in Si/SiGe/Si heterostructure bipolar transistors (HBTs) for gigahertz bandwidth communications.[2] For these applications, it is advantageous to incorporate metal silicide thin films so as to increase device drive current and to enhance the speed of an electronic circuit.[3-5] Ni germanosilicides formed on heavily doped SiGe substrates have been studied and shown to possess smooth interface at low processing temperature with excellent reverse leakage behavior.[6]

Rare-earth silicides have several advantages, including low formation temperature, low Schottky barrier height, ϕ_{Beff}, on n-type silicon compared to other metal silicide/n-Si systems (~0.3 eV vs ~0.65 eV for $ErSi_{2-x}$ and NiSi, respectively.[3] In addition, they can be epitaxially grown on Si(001) with a high crystallographic quality, which results in greater morphological stability and homogeneous Schottky barriers.[7,8]

The formation of erbium silicide on Si has been reported to result in microstructural defects, such as pits, pinholes, and pyramids, which result in degraded silicide/silicon interfaces, which may cause increasing leakage currents.[7,9,10] However, research on the solid phase reaction between erbium and silicon germanium have been limited. Travlos et al. have reported the material properties of epitaxial erbium silicide formed on Ge-implanted silicon as well as strained and relaxed $Si_{1-x}Ge_x$.[11,12] In this paper, we report the formation of epitaxial Er-germanosilicide films fabricated by rapid thermal annealing (RTA) of thin Er films on lightly doped p-$Si_{1-x}Ge_x(001)$ (x = 0–0.3) substrates at temperatures of 500–700°C. Materials characterization was conducted using two-dimensional (2D) X-ray diffraction (XRD), cross-sectional transmission electron microscopy (XTEM), and secondary ion mass spectroscopy (SIMS). Electrical measurements were performed on Er-germanosilicided Schottky diodes to elucidate the junction characteristics of erbium germanosilicide/$Si_{1-x}Ge_x$ interface.

Experimental

p-Doped relaxed $Si_{1-x}Ge_x$ virtual wafers [1 μm relaxed $Si_{1-x}Ge_x$ layers were grown on 2 μm thick $Si_{1-x}Ge_x$ graded layer on Si(001)] with a Ge atomic percentage of 0–30% were used as starting substrates. The wafers were cleaned using 1:4 H_2O_2:H_2SO_4 for 3 min, then dipped in dilute HF for 1 min prior to the deposition of a 50 nm thick erbium film at room temperature in a dc magnetron-sputtering chamber with a base pressure of 3×10^{-7} Torr. In some samples, a contact mask with 1 mm diameter circular holes was used as a physical barrier for selective erbium deposition during the sputter deposition process. The Er deposition was followed by a sequential deposition without breaking vacuum of 50 Å Ti and 200 Å TiN double capping layer, which serves to minimize oxidation. RTA was then carried out with an XM80 rapid thermal annealing system using an optimized condition of 500–700°C in a N_2 ambient for 60 s. A 2000 Å Au was deposited on the back side of the wafers with circular Er-silicide dots to form ohmic contact for electrical measurements.

Results and Discussion

The phases of the Er-silicide films formed were identified using X-ray diffraction [Bruker D8 general area detector diffraction system (GADDS) equipped with a two-dimensional detector]. Figure 1 shows typical two-dimensional (2D) θ – 2θ XRD patterns obtained

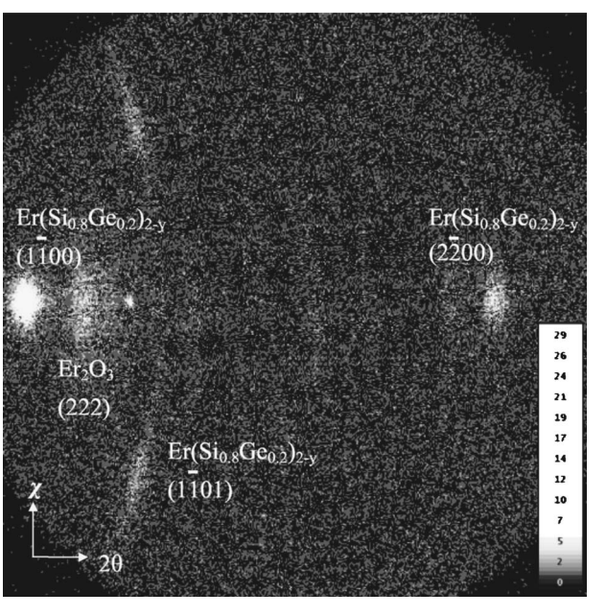

Figure 1. X-ray diffraction GADDS (general area detector diffraction system) scan of $Er(Si_{0.8}Ge_{0.2})_{2-y}/Si_{0.8}Ge_{0.2}(100)$ samples after RTA 600°C/60 s.

[z] E-mail: ejtan@ntu.edu.sg

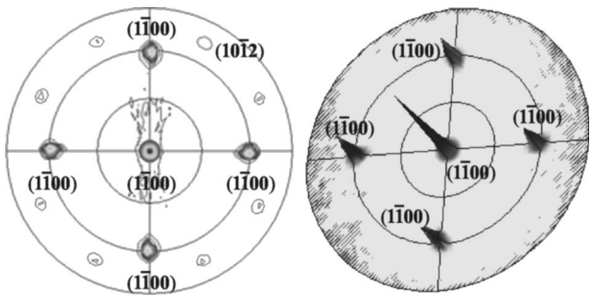

Figure 2. Two and three dimensional pole figure XRD scan of $Er(Si_{0.8}Ge_{0.2})_{2-y}/Si_{0.8}Ge_{0.2}(100)$ centered at the $Er(Si_{1-x}Ge_x)_{2-y}(1\bar{1}00)$ 2θ peak at 27°.

for Er films deposited on $Si_{0.8}Ge_{0.2}(001)$ after RTA at 600°C for 60 s [similar 2D XRD patterns were obtained for Er films on Si(001), $Si_{0.9}Ge_{0.1}(001)$, and $Si_{0.7}Ge_{0.3}(001)$]. Each pattern, i.e., Debye diffraction ring, is a plot of diffraction intensity for a particular diffraction angle 2θ (*x*-axis) with χ (*y*-axis). High intensity and well-defined spots, either located in the center of the Debye diffraction ring (i.e., $\chi = 0°$) or off-center positions, symmetrically, are due to diffractions from highly textured or even epitaxial film, whereas polycrystalline film would be typified by rings with uniformly distributed intensity.

Figure 1 shows the $(1\bar{1}00)$, $(2\bar{2}00)$, and $(1\bar{1}01)$ peaks of AlB2 hexagonal erbium disilicide, indicating that the germanosilicide phase is $Er(Si_{1-x}Ge_x)_{2-y}$ ($x = 0.2$). The observation of the 2D XRD patterns identical to that from Er film on Si(001) substrate, coupled with pole figure analysis of the same figure (see Fig. 2), further indicates that the $Er(Si_{1-x}Ge_x)_{2-y}$ films are also epitaxial, as in the case of $ErSi_{2-x}$ films formed on Si(001) [10] with orientation relationships $Er(Si_{1-x}Ge_x)_{2-y}(1\bar{1}00)[0001] \parallel Si_{1-x}Ge_x(001)[110]$. The fourfold symmetry of the $(1\bar{1}00)$ poles, rather than the twofold symmetry expected if the $Er(Si_{1-x}Ge_x)_{2-y}$ were a single crystal, confirms that the $Er(Si_{1-x}Ge_x)_{2-y}$ film contains both regions where the [0001] (i.e., *c*-axis) is parallel to Si [110] and where it is parallel to Si$[1\bar{1}0]$ (i.e., also containing grains with orientation relationship $Er(Si_{1-x}Ge_x)_{2-y}(1\bar{1}00)[0001] \parallel Si_{1-x}Ge_x(001)[1\bar{1}0]$), in agreement with the previous reports on epitaxial erbium disilicide on Si(001).[10,13] The d-spacing of the $(1\bar{1}00)$ planes for $Er(Si_{1-x}Ge_x)_{2-y}$ ($x = 0$–0.3) (extracted from the experimental 2θ values) are 0.48–0.87% larger than the corresponding values for the relaxed $Er(Si_{1-x}Ge_x)_{2-y}$ ($x = 0$–0.3) film. The relaxed $Er(Si_{1-x}Ge_x)_{2-y}(1\bar{1}00)$ d-spacing was found by using Vegard's law for an ideal solid solution[14] [i.e., treating $Er(Si_{1-x}Ge_x)_{2-y}$ as a solid solution of $ErSi_{2-x}$ and $ErGe_{2-x}$] on the calculated d-spacing of $ErSi_{1.67}$ and $ErGe_{1.5}$.[15] The observation of larger d-spacing of the $(1\bar{1}00)$ planes from the θ − 2θ XRD measurement is certainly due to the presence of a biaxial and compressive strain in the epitaxial $Er(Si_{1-x}Ge_x)_{2-y}$ film [−2.7% for $ErSi_{2-x}$ [(Ref. 10)], which results in the increase of the d-spacing of the $Er(Si_{1-x}Ge_x)_{2-y}(1\bar{1}00)$ planes oriented parallel to the (001) Si substrate plane. Also observed in Fig. 2 are weak peaks of the orientation $Er(Si_{1-x}Ge_x)_{2-y}(10\bar{1}2) \times [01\bar{1}0] \parallel Si_{1-x}Ge_x(001)[010]$, which have also been observed for Er-germanide.[16]

Despite the use of the TiN/Ti capping layer, small traces of Er_2O_3 and $Er_2SiO_5/Er_2(SiGeO)_5$ are detected due the oxidation of the extremely reactive Er in the annealing ambient. However, it must be said that the samples showed a stronger $Er(Si_{1-x}Ge_x)_{2-y}$ $(1\bar{1}00)$ peak and greatly reduced Er_2O_3 and $Er_2SiO_5/Er_2(SiGeO)_5$ peaks

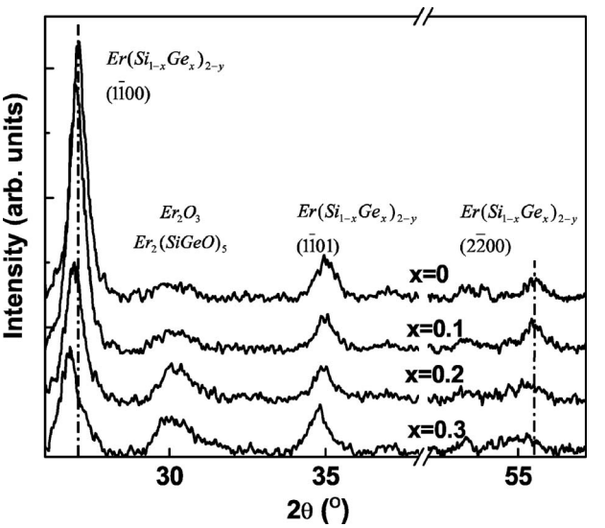

Figure 3. X-ray diffraction single crystal θ–2θ plots of $Er(Si_{1-x}Ge_x)_{2-y}$ samples with varying Ge concentrations. Dotted lines indicate the positions of the $Er(Si_{1-x}Ge_x)_{2-y}(1\bar{1}00)$ and $(2\bar{2}00)$ ($x = 0$) peaks, respectively.

compared to the samples without the TiN/Ti capping. In addition, it has been previously reported that Ti capped $Er/Si_{1-x}Ge_x$ ($x = 0.088$) samples have also shown suppression of Er_2SiO_5 XRD peaks and improvement in phase formation.[17]

Figure 3 shows the XRD 2θ plots of $Er(Si_{1-x}Ge_x)_{2-y}$ samples with Ge concentrations $x = 0$–0.3. The XRD plots show that there is a left shift of the $Er(Si_{1-x}Ge_x)_{2-y}(1\bar{1}00)(1\bar{1}00)$ peak position, which corresponds to an increasing spacing of the $Er(Si_{1-x}Ge_x)_{2-y}(1\bar{1}00)$ lattice planes, with increasing Ge concentration in SiGe substrate. The increase of lattice constants in $Er(Si_{1-x}Ge_x)_{2-y}$ is certainly due to the fact that AlB2 hexagonal erbium digermanide $ErGe_{2-x}$ has larger lattice constant $a = b = 3.889$ Å as compared to the corresponding value of $a = b = 3.798$ Å for AlB2 hexagonal erbium disilicide $ErSi_{2-x}$, in accordance with Vegard's law for ideal solid solution.

Figure 4 shows a XTEM micrograph of the Er-germanosilicided $Si_{1-x}Ge_x$ ($x = 0.2$) films annealed at 600°C. From the results (see Fig. 4a, top micrograph taken at a lower magnification), it is observed that the Er-germanosilicided film is uniform with a thickness of ~85 nm (with 16 nm TiN capping). The Er-germanosilicide/$Si_{0.8}Ge_{0.2}$ interface is smooth with no evidence of agglomeration or Ge segregation, which is typically observed for Ni germanosilicided films annealed at >500°C.[18] The high-resolution TEM micrograph of the same sample (Fig. 4b, bottom micrograph) shows that the Er-germanosilicided film is indeed epitaxial to the underlying Si0.8$Ge_{0.2}$ substrate: almost a 1:1 relationship is observed for the $Er(Si_{1-x}Ge_x)_{2-y}(1\bar{1}01)$ and Si(111) lattice planes across the interface as expected for $Er(Si_{1-x}Ge_x)_{2-y}(1\bar{1}00)[0001] \parallel Si_{1-x}Ge_x(001)[110]$ orientation relationship. The TEM/energy dispersive X-ray (EDX) compositional analysis shows that the ratio of Si/Ge at the substrate regions labeled 1 is around 81.3:18.7 (±3%) while the ratio of Er-:Si:Ge at the Er-germanosilicide regions labeled 2 is around 31.4:56.4:12.3 (±6%). It is noted that the Si/Ge ratio (~4.58) in the $Er(Si_{1-x}Ge_x)_{2-y}$ layer is essentially equal to that in the underlying SiGe substrate, i.e., ~4.35, indicating that the Si/Ge ratio is maintained in the silicide layer after the reaction of Er with the $Si_{0.8}Ge_{0.2}$ substrate.

Figure 5 shows the secondary ion mass spectroscopy (SIMS) depth profiles of the Er-germanosilicide samples with Ge concentrations ($x = 0.1$–0.3). Figure 5 shows that layered structures of

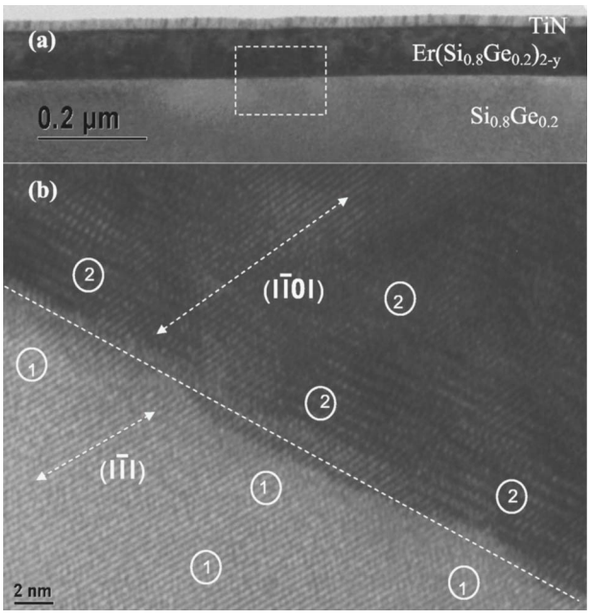

Figure 4. XTEM micrographs of the $Er(Si_{0.8}Ge_{0.2})_{2-y}/Si_{0.8}Ge_{0.2}(100)$ interface. (a) The top XTEM micrograph shows the germanosilicide/SiGe interface at low magnification. (b) The bottom XTEM micrograph shows the bright field HRTEM of the interface indicated by the dotted white box in (a). TEM/EDX analysis was done on the circled regions.

$Er(Si_{1-x}Ge_x)_{2-y}$ of similar thicknesses were formed in all three samples, which correspond to the relative flat portions of the erbium, silicon, and germanium signals. To investigate the uniformity of the $Er(Si_{1-x}Ge_x)_{2-y}$ layers, we calculated the ratio of Si to Er and found that the Si count is constant from the $Er(Si_{1-x}Ge_x)_{2-x}$/Si interface toward the surface until ~50 nm from the surface, whereby the Si counts decreases by 0.52%/nm. This decrease occurs until ~25 nm from the surface, whereby the interference of the oxygen and titanium signals interferes with the calculation. The decreasing Si count from 50 nm onward toward the surface can be understood on the basis that Si/Ge is the diffusing species in the Er to $Si_{1-x}Ge_x$ solid-state reaction. For a RTA time of 60 s, the $Er(Si_{1-x}Ge_x)_{2-x}$ film is unable to achieve its preferred stoichiometry $[Er(Si_{1-x}Ge_x)_{1.67}]$,

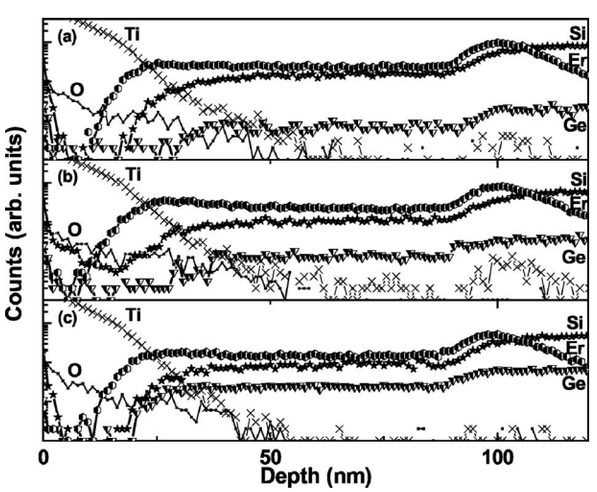

Figure 5. SIMS depth profile of $Er(Si_{1-x}Ge_x)_{2-y}/Si_{1-x}Ge_x(100)$ samples after RTA 600°C/60 s in N_2 ambient using an ION-TOF SIMS with a Ga ion beam. (a) $x = 0.1$, (b) $x = 0.2$, and (c) $x = 0.3$.

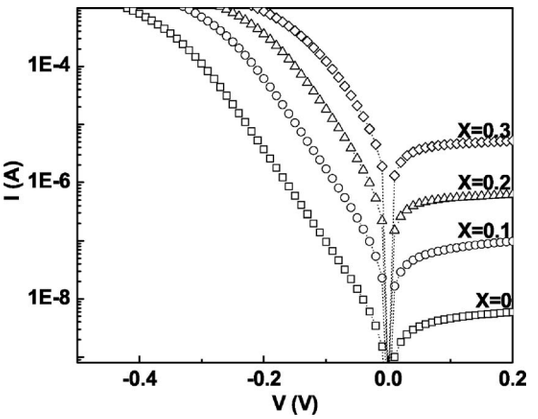

Figure 6. Current-voltage characteristics of TiN/Ti capped $Er(Si_{1-x}Ge_x)_{2-y}$ diodes ($x = 0$–0.3) measured at 25°C.

hence, the Si deficiency nearer to the surface. The results in Fig. 5 also show that oxygen penetration was effectively suppressed and mostly confined at the TiN/Ti capping layer, illustrating that the TiN/Ti capping layer is effective in blocking oxygen diffusion during RTA.

The *I-V* characteristics of the formed Er-germanosilicided diodes ($x = 0.1$–0.3) as well as the control diode [i.e., $ErSi_{2-x}$/p-Si(001)] were measured, as shown in Fig. 6. As shown, both reverse current and forward saturation current increase with increasing Ge content in the substrate. Because typical ideality factors obtained from these diodes are 1.05–1.15, which is much smaller than 2 but close to 1, the increase in the reverse current and forward saturation current must be due to the reduction in the Schottky barrier height ϕ_{Bpeff} due to the increasing Ge content.

In order to experimentally determine ϕ_{Bpeff}, temperature-dependent *I-V* curves were measured on these diodes. The associated saturation current I_{sat} values were obtained by extrapolating the $\log(I/[1 - \exp(-eV/kT)])$ vs V curve to $V = 0$ (see Fig. 7a, as an example). From the slopes of Richardson plots (shown in Fig. 7b), i.e., the plot of $\ln(I_{sat}/T^2)$ against $1/T$, the effective barrier height ϕ_{Bpeff} values were calculated. Figure 8 shows the actual barrier height ϕ_{Bp} values after taking into account image-force–induced barrier lowering $\Delta\Phi$ by using the well-known relation[19]

$$\Delta\Phi = \sqrt{\frac{qE}{4\pi\varepsilon_s}} \qquad [1]$$

with $E = \{[2qN_a/\varepsilon_s][V_{bi} - V - (kT/q)]\}^{1/2}$ as the maximum electric field, ε_s is the permittivity determined from Ref. 14, V_{bi} is the built-in potential, and N_a is the acceptor concentration both determined by capacitance-voltage measurements. By assuming the bandgap $E_g = q(\phi_{Bp} + \phi_{Bn})$ and using the relationship, $E_g = 1.12 - 0.41x + 0.008x^2$ eV,[14] between E_g and Ge content x in $Si_{1-x}Ge_x$, the barrier height for electron injection, i.e., ϕ_{Bn}, were also calculated.

It is known that in $Si_{1-x}Ge_x$, the reduction of bandgap E_g with increasing Ge content x is purely due to the change (i.e., moving up) of valence bandedge E_v position as the conduction bandedge position, E_c changes only slightly with respect to x (note: E_c position relative to vacuum level is related to x by $E_c = -4.05 + 0.05x$).[20] It was also found that the workfunction of Er-germanide is ~0.3 eV larger than that of Er-silicide,[21] suggesting a deeper Fermi-level E_{fm} position (relative to vacuum level) for $Er(Si_{1-x}Ge_x)_{2-y}$ as compared to $ErSi_{2-x}$ [provided that the workfunction of $Er(Si_{1-x}Ge_x)_{2-y}$ varies monotonically with x]. As the barrier height for hole ϕ_{Bp} is more or less the difference between metal Fermi level E_{fm} and E_v, it is appropriate to assume that the reduction in ϕ_{Bp} with increasing x is

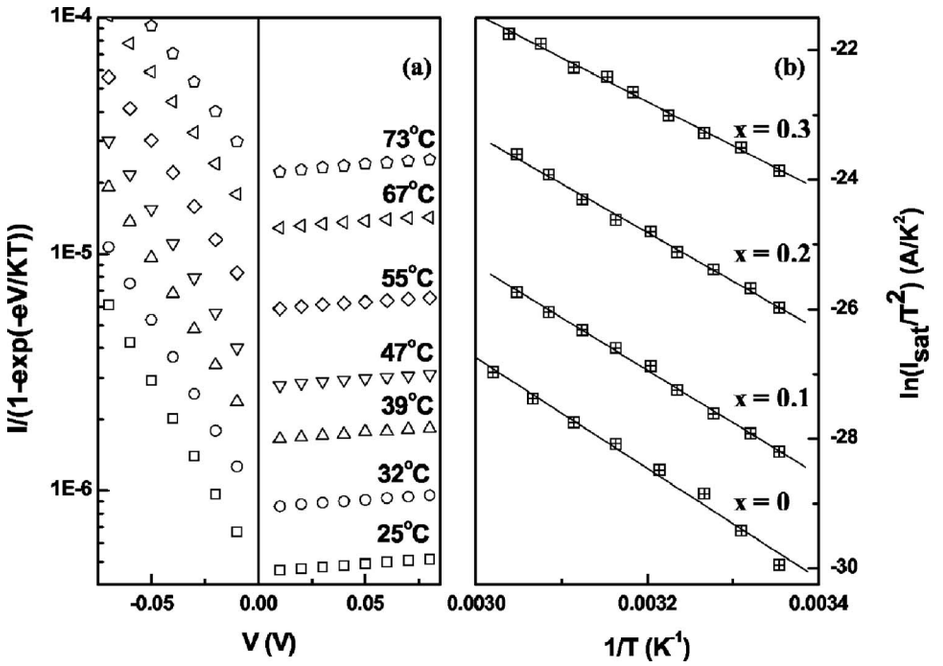

Figure 7. (a) Temperature dependent $\log(I/\{1 - \exp[-(eV/kT)]\})$ *I-V* plots measured on $Er(Si_{1-x}Ge_x)_{2-y}$ diodes ($x = 0.2$) with typically low leakage currents. (b) Richardson's plot for $Er(Si_{1-x}Ge_x)_{2-y}$ diodes ($x = 0$–0.3).

mainly due to the change (i.e., moving up) of E_v position, and, to a certain extent, the change (i.e., moving down) of E_{fm} position. The slight increase in ϕ_{Bn} with x is largely due to the change in E_{fm} position with additional contribution by the change (i.e., moving up) in E_c position (note: ΔE_c is only 15 meV for $x = 0.3$ while $\Delta q\phi_{Bn} \cong 52$ meV). The electron barrier height of $NiSi_{1-x}Ge_x$ ($x = 0$, 0.3) is also plotted in Fig. 8 and, as can be seen, is larger that the electron barrier height of $Er(Si_{1-x}Ge_x)_{2-y}$ by $\sim$0.3 eV. The larger barrier height results in a larger contact resistance R_{co} for $NiSi(NiSi_{1-x}Ge_x)$/n-Si(SiGe) systems (e.g., source-drain contact of N-MOS transistors, etc.). Note that a 0.3 eV larger barrier height would result in a larger R_{co} by $\sim$1 order of magnitude considering a semiconductor doping concentration of $\sim 10^{20}$ cm^{-3}.[23]

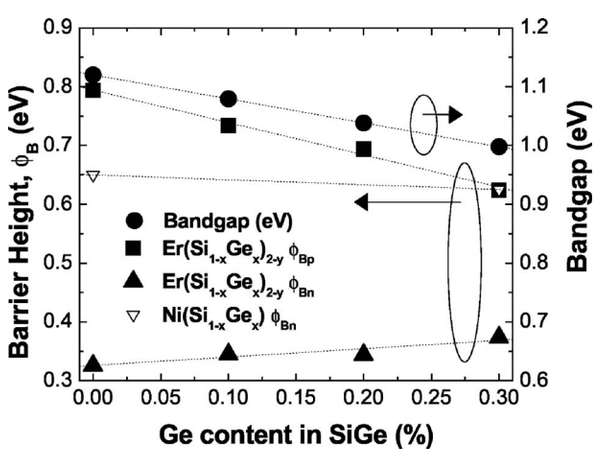

Figure 8. Schottky barrier height to holes, ϕ_{Bp}, and electrons, ϕ_{Bn}, of the $Er(Si_{1-x}Ge_x)_{2-y}$/p-$Si_{1-x}Ge_x$ diodes ($x = 0$–0.3), and Schottky barrier height to electrons of $NiSi_{1-x}Ge_x$/n-$Si_{1-x}Ge_x$ diodes ($x = 0,0.3$) from Ref. 22. Varying bandgap, E_g, with Ge concentration is also plotted. ϕ_{Bn} calculated using the relation $E_g = q(\phi_{Bp} + \phi_{Bn})$.

Conclusion

We have fabricated epitaxial growth of erbium germanosilicide on relaxed $Si_{1-x}Ge_x$ ($x = 0$–0.3) substrates with orientation relationship $Er(Si_{1-x}Ge_x)_{2-y}(1\bar{1}00)[0001] \parallel Si_{1-x}Ge_x(001)[110]$ or $Er(Si_{1-x}Ge_x)_{2-y}(1\bar{1}00)[0001] \parallel Si_{1-x}Ge_x(001)[\bar{1}10]$. Electrical characteristics indicate that the Er-germanosilicide/$Si_{1-x}Ge_x$ interfaces are near ideal with decreasing Schottky barrier height, ϕ_{Bp} from 0.79 to 0.62 eV of $Er(Si_{1-x}Ge_x)_{2-y}$/p-$Si_{1-x}Ge_x$ (100) with increasing Ge (from 0–30%). This implies a slight increase in its barrier height for electrons, ϕ_{Bneff}, from 0.33 to 0.37 eV. Thus Er-germanosilicide can potentially be used as a high-quality contact to $Si_{1-x}Ge_x$ for advanced nanodevice applications, including Si-based optoelectronic devices, Si/SiGe HBTs, and CMOS applications.

Acknowledgments

E.J.T. would like to acknowledge Systems on Silicon Manufacturing Co., Private Ltd., (SMMC) and Institute of Materials and Research Engineering (IMRE), Singapore, for financial support. This work was financed in part by A*STAR grant no. 0321010007 and 0421140049.

SSMC and IMRE assisted in meeting the publication costs of this aricle.

References

1. I. Aberg, C. N. Chleirigh, and J. L. Hoyt, *IEEE Trans. Electron Devices*, **53**, 1021 (2006).
2. J. S. Weiner, A. Leven, V. Houtsma, Y. Baeyens, Y. K. Chen, P. Paschke, Y. Yang, J. Frackoviak, W. J. Sung, A. Tate, et al., *IEEE J. Solid-State Circuits*, **38**, 1512 (2003).
3. K. Maex and M. van Rossum, *Properties of Metal Silicides*, INSPEC, IEE, London (1995).
4. T. L. Lee, J. W. Lee, M. C. Lee, T. F. Lei, and C. L. Lee, *Electrochem. Solid-State Lett.*, **6**, G66 (2003).
5. R. Nath and M. Yeadon, *Electrochem. Solid-State Lett.*, **7**, G231 (2003).
6. J. Liu and M. C. Ozturk, *IEEE Trans. Electron Devices*, **52**, 1535 (2005).
7. J. A. Knapp, S. T. Picraux, C. S. Wu, and S. S. Lau, *J. Appl. Phys.*, **58**, 3747 (1985).
8. R. T. Tung, *Phys. Rev. B*, **45**, 13509 (1992).
9. E. J. Tan, K. L. Pey, D. Z. Chi, P. S. Lee, and L. J. Tang, *IEEE Electron Device Lett.*, **27**(2), 93 (2006).
10. E. J. Tan, M. Bouville, D. Z. Chi, K. L. Pey, P. S. Lee, D. J. Srolovitz, and C. H. Tung, *Appl. Phys. Lett.*, **88**, 021908 (2006).

11. A. Travlos, G. Apostolopoulos, N. Boukos, Ch. Katiniotis, and D. Tsamakis, *Mater. Sci. Eng., B*, **89**, 382 (2002).
12. A. Travlos, N. Boukos, G. Apostolopoulos, C. J. Aidinis, and L. Bischoff, *Nucl. Instrum. Methods Phys. Res. B*, **196**, 174 (2002).
13. A. Travlos, N. Salamouras, and E. Flouda, *Appl. Surf. Sci.*, **120**, 355 (1997).
14. E. Kasper, *Properties of Strained and Relaxed Silicon Germanium*, EMIS Datareviews Series No. 12, INSPEC, IEE, London (1995).
15. Joint Committee for Powder Diffraction Standards, Powder Diffraction File No. 47-1285, and 18-0484, JCPDS International Center Diffraction Data, Swarthmore, PA (1976).
16. S. L. Liew, B. Balakrisnan, C. S. Ho, O. Thomas, and D. Z. Chi, *J. Electrochem. Soc.*, **154**, h9 (2006).
17. Q. F. D. Yiew, Y. Setiawan, P. S. Lee, and D. Z. Chi, *Thin Solid Films*, **504**, 91 (2006).
18. K. L. Pey, W. K. Choi, S. Chattopadhyay, H. B. Zhao, E. A. Fitzgerald, D. A. Antoniadis, and P. S. Lee, *J. Vac. Sci. Technol. A*, **20**, 1903 (2002).
19. S. M. Sze, *Physics of Semiconductor Devices*, 2nd ed., Wiley, New York (1981).
20. *Properties of Advanced Semiconductor Materials: GaN, AlN, InN, BN, SiC, and SiGe*, M. E. Levinshtein, S. L. Rumyantsev, and M. S. Shur, Editors, Wiley, New York (2001).
21. Y. Tsuchiya, M. Koyoma, J. Koga, and A. Nishiyama, *Ext. Abstr. Solid State Dev. Mat. Conf.*, **2005**, 844.
22. L. J. Jin, Ph.D. Thesis, Singapore-MIT Alliance, National University of Singapore, Singapore (2005).
23. K. K. Ng and R. Liu, *IEEE Trans. Electron Devices*, **37**, 1535 (1990).